ULTRASOUND ELASTOGRAPHY OF BREAST CANCER-RELATED LYMPHEDEMA

H. S. Hashemi[1] *S. Fallone*[2,3] *M. Boily*[2,4] *A. Towers*[5,6] *R. D. Kilgour*[2,3] *H. Rivaz*[2,7]

[1] Department of Electrical and Comuter Engineering, University of British Columbia
[2] PERFORM Centre, Concordia University
[3] Department of Exercise Science, Concordia University
[4] Department of Radiology, McGill University Health Centre (MUHC)
[5] Department of Oncology, McGill University
[6] McGill Lymphedema Research Program
[7] Department of Electrical and Comuter Engineering, Concordia University

ABSTRACT

Accurate methods of staging breast cancer-related lymphedema (BCRL) are lacking and have become a major cause of concern among clinicians. However, with the application of novel techniques in ultrasound elastography, clinicians may be able to better assess BCRL and provide targeted treatments to reduce the progression of this condition. In this paper, we propose to use strain images estimated using quasi-static ultrasound elastography techniques to investigate its usefulness in staging lymphedema. We further propose a novel approach for estimating the strain images from two frames of ultrasound data. Using data collected from two patients with lymphedema, we show that strain images can potentially be used to accurately diagnose lymphedema. Using phantom and *in-vivo* data, we further show that the proposed strain estimation technique substantially outperforms previous work.

Index Terms— Breast Cancer, Lymphedema, Ultrasound elastography.

1. INTRODUCTION

Failure of the lymphatic system results in tissue inflammation, adipose tissue hypertrophy, and fibrosis [1]. Collectively, these pathological adaptations result from the condition known as lymphedema. Primary or innate lymphedema can occur due to anomalous development of the lymph nodes or lymphatic vessels [2], and secondary lymphedema is normally caused by trauma, infection, tumor infiltration, surgical dissection of lymph nodes, or radiation therapy [3]. Secondary lymphedema is substantially more common than the primary condition. Most cases of upper-extremity lymphedema emerge after breast cancer surgery and radiation treatment [1]. Lymphedema is often categorized into four stages [4]. In this study, we focus on Stage 2 lymphedema of the arm following breast cancer surgery or radiation. At Stage 2 or moderate lymphedema, the tissue underneath the skin such as subcutaneous fat and skeletal muscle becomes harder and thicker with evident inflammation and swelling of the limb. The progress can be controlled with treatment, but there is usually no remedy for the tissue damage.

Early detection and staging of lymphedema are critical for choosing the appropriate treatment and for monitoring the prognosis. Ultrasound imaging can be used to investigate the changes in the subcutaneous tissue that are associated with lymphedema, which include increased thickness of the dermis, a shift from hypo- to hyperechogenicity of the subcutis, and fluid retention located in the dermis, interlobular space, and superficial fascia [5]. However, ultrasonic appearance of these changes can be negligible and hard to detect. Therefore, changes in mechanical properties are explored in [6, 7, 8] by focusing on poroelasticity. Recent work has also applied compression with the ultrasound probe, and used B-mode ultrasound to manually measure tissue thickness [3, 9, 10, 11]. This measurement can be performed with greater accuracy by using the Radio-Frequency (RF) data instead of the B-mode image, and by using Time Delay Estimation (TDE) methods that are widely used in quasi-static ultrasound elastography [12, 13, 14, 15, 16]. Another difficulty in manually measuring the thickness of skin lies in normalization of the applied pressure: when comparing the thickness of the two arms, the applied pressure should be equal. Therefore, new research has proposed to use pressure sensors to generate equal pressure in both arms [17]. In this work, we propose to use an acoustic gel pad to normalize the applied pressure on the tissue. In addition to normalizing the applied pressure, the gel pad will increase the resolution of ultrasound data at the skin.

In this study, we introduce a novel method for characterizing tissue properties in women who have been diagnosed with Stage 2 breast cancer-related lymphedema (BCRL). This novel method involves the calculation of TDE using RF data, and to use TDE to calculate the strain values for the subcu-

taneous fat and skeletal muscle layers in the affected and unaffected arms. To the best of our knowledge, this is the first time that this approach is used in studying the effect of lymphedema on tissue property characteristics. More specifically, the contributions of this work are:

1. Proposing a novel method for TDE for quasi-static elastography using the second-order Taylor expansion
2. Proposing a novel method for optimization of the cost function based on Efficient Second-order minimization (ESM) [18]
3. Introducing a novel metric based on ultrasound elastography for comparing affected and unaffected arms in patients with lymphedema

The new method is based on our recent work entitled GLUE [19]: GLobal Ultrasound Elastography. We introduce two novel techniques to substantially improve GLUE. We therefore call our method GLUE2, and we show that it substantially outperforms GLUE using results on a tissue-mimicking phantom and $in-vivo$ patient data.

2. METHODS

We now briefly describe the closely related previous work of GLUE [19], followed by a presentation of GLUE2.

2.1. GLobal Ultrasound Elastography (GLUE)

Let I_1 and I_2 be images of size $m \times n$ obtained before and after some deformation. Also, let $a_{i,j}$ and $l_{i,j}$ denote be axial and lateral displacements of sample (i,j), where $i = 1 \cdots m$ and $j = 1 \cdots n$. First, an estimate of the displacement estimates in the axial ($a_{i,j}$) and lateral ($l_{i,j}$) directions are calculated using the Dynamic Programming Analytic Minimization (DPAM) method [20]. The goal of GLUE is to find subsample $\Delta a_{i,j}$ and $\Delta l_{i,j}$ displacements such that the duple $(a_{i,j} + \Delta a_{i,j}, l_{i,j} + \Delta l_{i,j})$ provides accurate axial and lateral displacement estimates for all the samples of the RF frame simultaneously. The GLUE cost function is defined as:

$$C(\Delta a_{1,1}, \cdots, \Delta a_{m,n}, \Delta l_{1,1}, \cdots, \Delta l_{m,n}) = \sum_{j=1}^{n} \sum_{i=1}^{m} \{D(i,j) + R(i,j)\} \quad (1)$$

where the data term D and the regularization term R are:

$$D(i,j) = [I_1(i,j) - I_2(i + a_{i,j} + \Delta a_{i,j}, j + l_{i,j} + \Delta l_{i,j})]^2, \quad (2)$$

$$\begin{aligned} R = & \\ & \alpha_1 (a_{i,j} + \Delta a_{i,j} - a_{i-1,j} - \Delta a_{i-1,j})^2 \\ & + \beta_1 (l_{i,j} + \Delta l_{i,j} - l_{i-1,j} - \Delta l_{i-1,j})^2 \\ & + \alpha_2 (a_{i,j} + \Delta a_{i,j} - a_{i,j-1} - \Delta a_{i,j-1})^2 \\ & + \beta_2 (l_{i,j} + \Delta l_{i,j} - l_{i,j-1} - \Delta l_{i,j-1})^2, \end{aligned} \quad (3)$$

and α and β are regularization weights in axial and lateral directions respectively.

2.2. Incorporation of the Second-Order Taylor Expansion into the Cost Function

GLUE uses the first order Taylor expansion to make the cost function in Eq. 1 quadratic. Including higher order derivatives for the data term can improve the accuracy of displacement estimation. However, doing so will make the derivative of Eq. 11 nonlinear, and therefore the optimization problem becomes intractable given that this equation has millions of variables.

We propose a novel technique to incorporate the second-order Taylor expansion into the cost function while keeping the problem computationally efficient. Our cost function is

$$C = \sum_{j=1}^{n} \sum_{i=1}^{m} \{w(i,j) D(i,j) + R(i,j)\} \quad (4)$$

where w is the weight of each data term:

$$w(i,j) = \frac{1}{\epsilon + |I"(i,j)_{2,a}| + |I"(i,j)_{2,l}|} \quad (5)$$

and ϵ is a small positive constant to prevent the denominator to become zero, and $|I"_{2,a}|$ and $|I"_{2,l}|$) are the absolute values of second-order derivatives in the axial and lateral directions respectively. The introduced weight r reduces the contribution of regions of the RF-data with high second-order derivatives. Therefore, we incorporate second-order derivatives while maintaining the quadratic form of the cost function.

2.3. Efficient Second-order Minimization (ESM)

The second technical contribution of this work is that we utilize the Efficient Second-order Minimization (ESM) optimization method [18] for the first time for TDE. ESM is shown to have superior convergence properties [21, 22, 23] compared to the asymmetric Gauss-Newton optimization method used in [19].

Let $p = (i + a_{i,j}, j + l_{i,j})$ denote a vector containing the coordinate of a pixel after an approximate displacement $(a_{i,j}, l_{i,j})$, and consider $p + \Delta p = (i + a_{i,j} + \Delta a_{i,j}, j + l_{i,j} + \Delta l_{i,j})$ as its refined location after a small displacement estimate $(\Delta a_{i,j}, \Delta l_{i,j})$. Thus, for a second-order Taylor series of I_2 we have:

$$\begin{aligned} & I_2(p + \Delta p) = I_2(p) + I'_{2,a}(p) \Delta a_{i,j} + I'_{2,l}(p) \Delta l_{i,j} + \\ & \tfrac{1}{2} I"_{2,a}(p) \Delta a_{i,j}^2 + \tfrac{1}{2} I"_{2,l}(p) \Delta l_{i,j}^2 + \chi(\Delta a_{i,j}^3, \Delta l_{i,j}^3) \end{aligned} \quad (6)$$

where $\chi(\Delta a_{i,j}^3, \Delta l_{i,j}^3)$ is a third-order reminder. Similarly, we can write the Taylor series of the derivatives $I'_{2,a}(p + \Delta p)$ and $I'_{2,l}(p + \Delta p)$ about point p:

$$I'_{2,a}(p + \Delta p) = I'_{2,a}(p) + I"_{2,a}(p) \Delta a_{i,j} + \chi(\Delta a_{i,j}^2), \quad (7)$$

$$I'_{2,l}(p + \Delta p) = I'_{2,l}(p) + I"_{2,l}(p) \Delta l_{i,j} + \chi(\Delta l_{i,j}^2) \quad (8)$$

Inserting Eq. 7, and 8 in Eq. 6 to eliminate $I"_{2,a}(p)$ and $I"_{2,l}(p)$ leads to:

$$I_2(p+\Delta p) = I_2(p) + \tfrac{1}{2}\{I'_{2,a}(p) + I'_{2,a}(p+\Delta p)\}\Delta a_{i,j} + \tfrac{1}{2}\{I'_{2,l}(p) + I'_{2,l}(p+\Delta p)\}\Delta l_{i,j} \tag{9}$$

Using similarity of RF data approximation i.e. $I'_{2,a}(p+\Delta p) \approx I'_{1,a}(p)$ and $I'_{2,l}(p+\Delta p) \approx I'_{1,l}(p)$, and inserting in Eq. 9, gives a second order approximation of I_2 in $(p+\Delta p)$:

$$I_2(p+\Delta p) = I_2(p) + \tfrac{1}{2}\{I'_{2,a}(p) + I'_{1,a}(p)\}\Delta a_{i,j} + \tfrac{1}{2}\{I'_{2,l}(p) + I'_{1,l}(p)\}\Delta l_{i,j} \tag{10}$$

Utilizing Eq. 10 in our cost function of Eq. 4, we have:

$$C(\Delta a_{1,1}, \cdots, \Delta a_{m,n}, \Delta l_{1,1}, \cdots, \Delta l_{m,n}) = \sum_{j=1}^{n}\sum_{i=1}^{m}\{r_{i,j}[I_1(i,j) - I_2(i+a_{i,j}, j+l_{i,j}) - \tfrac{1}{2}(I'_{2,a}(p) - I'_{1,a}(p))\Delta a_{i,j} - \tfrac{1}{2}(I'_{2,l}(p) - I'_{1,l}(p))\Delta l_{i,j}]^2 + R(i,j)\} \tag{11}$$

where $I'_{1,a}$, $I'_{2,a}$, $I'_{1,l}$ and $I'_{2,l}$ are calculated at the point $(i + a_{i,j}, j + l_{i,j})$. This equation is a quadratic equation with respect to the unknowns $\Delta a_{i,j}$ and $\Delta l_{i,j}$, and therefore can be efficiently optimized by setting its derivative with respect to the unknowns to zero.

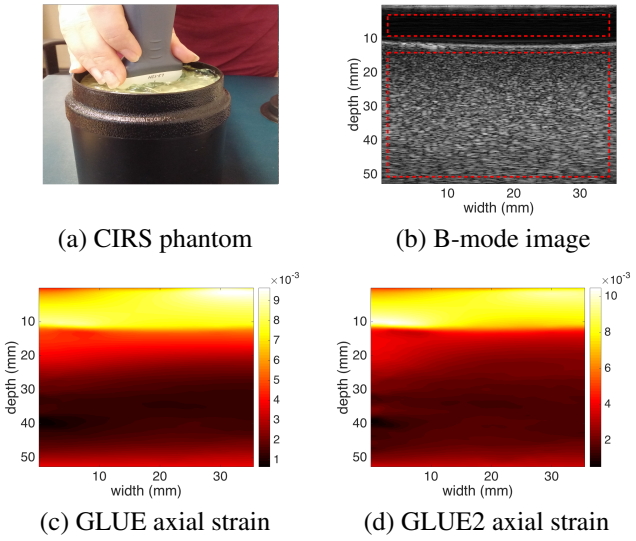

(a) CIRS phantom (b) B-mode image

(c) GLUE axial strain (d) GLUE2 axial strain

Fig. 1. Results of the data collected from the CIRS phantom.

3. RESULTS

RF data is collected with an Alpinion E-Cube system (Bothell, WA) using the L3-8 transducer at the centre frequency of 10 MHz and the sampling rate of 40 MHz from a tissue mimicking phantom and two patients with Stage 2 lymphedema. The patient data is collected at McGill University Health Centre (MUHC) Lymphedema clinic. The study was approved by MUHC Ethics Board, and both subjects provided written consent. We use the unitless metric strain ratio (SR) to quantitatively compare the results of the affected and unaffected limb. SR is calculated for the subcutaneous fat and skeletal muscle tissue using the following equations:

$$\mathrm{SR_f} = \frac{\bar{S_f}}{\bar{S_g}},\ \mathrm{SR_m} = \frac{\bar{S_m}}{\bar{S_g}} \tag{12}$$

where $\bar{S_g}$, $\bar{S_f}$ and $\bar{S_m}$ are the spatial average of the strain in the gel pad, subcutaneous fat and muscle. All the spatial average values are calculated within a window of size 8mm×3mm in the corresponding regions of the strain image. Note that the same tissue can have different strain values depending on the compression applied. The division by the average strain of the gel pad normalizes the strain value and makes it independent from the applied compression.

3.1. Results on Phantom Data

For experimental validation, RF data is acquired from a CIRS elastography phantom (Norfolk, VA) with a Young's Elasticity Modulus of 7KPa (Figure 1). The probe is hand-held as shown in (a), and the gel pad is placed below the probe (not clearly visible in (a)). The phantom is uniform, which leads to an approximately uniform strain as depicted in (c) & (d). The strain estimate of GLUE2, shown in part (d), is more uniform than (c) as expected. To perform quantitative comparison of GLUE and GLUE2, the unitless metrics signal to noise ratio (SNR) and contrast to noise ratio (CNR) [12] are calculated using the red rectangles marked in (b). The SNR values for GLUE and GLUE2 are 17.50 and 17.76, and the CNR values are 3.81 and 3.92 respectively. These numbers illustrate that GLUE2 outperforms GLUE.

3.2. Results on Patient Data

The study population was composed of women with arm lymphedema resulting from breast cancer treatment. We placed the 6 following landmarks on both arms to mark the location of the data collection. Landmark locations are 20% the distance: between the styloid process of the pinkie and tip of it, between the styloid process of the pinkie and olecranon, between olecranon and styloid process of pinkie, between olecranon and acromioclavicular (AC) joint, between AC joint to olecranon, and finally 40% the distance of AC joint and olecranon.

Figure 2 shows the strain results of three landmarks for patient 1 in the affected arm using GLUE and GLUE2 methods. Each row represents a landmark on the patient arm. The windows show the location of the boxes used for calculating average strain and are placed on gel pad, fat, and muscular regions. The location of these windows is verified by a fellowship trained musculoskeletal radiologist (M. B.) specialized in ultrasound imaging. We calculated SR utilizing GLUE2 for 2 patients in all 6 landmark locations, and show the average results in every location in Table 1. The results show that SR has consistently higher values for the unaffected compared to

Table 1. SR values for the six landmark locations of the unaffected (U) and affected (A) arms.

Location	Fat		Muscle	
	U	A	U	A
Location 1	0.50	0.32	0.52	0.29
Location 2	0.31	0.12	0.66	0.27
Location 3	0.33	0.21	0.82	0.60
Location 4	0.31	0.19	0.75	0.52
Location 5	0.76	0.29	1.52	0.85
Location 6	1.27	0.85	1.95	0.93

Table 2. SR ratio of the unaffected arm divided by affected arm (U/A) for each landmark location. The maximum values are in bold font.

Location	Fat (U/A)	Muscle (U/A)	Sum
1	1.56	1.79	3.35
2	2.58	**2.44**	**5.02**
3	1.57	1.36	2.93
4	1.63	1.44	3.07
5	**2.62**	1.79	4.41
6	1.49	2.09	3.58

the affected arm, but a larger sample size is needed to draw statistical conclusions.

To compare the SR measurements at different locations, we divide the average SR values of the unaffected arm by the affected arm from Table 1, and show them in Table 2. The ratio is shown for the fat and and muscle tissue types. In these two women, the optimal locations for acquiring data to distinguish the affected from the unaffected arm are the landmark 2 and 5 for the subcutaneous fat and landmark 2 for the skeletal muscle area (Table 2). To obtain the overall best location, we add these two ratios at the fat and muscle regions, and show the results in the last column of Table 2. The values demonstrate that locations 2, 5 and 6 have the highest difference between the two arms. Data from more patients is needed to establish statistical significance.

Another interesting observation from this table is that subcutis fat provides the highest difference between the SR values of the affected and healthy arms with a very high ratio of 2.76. Furthermore, the average SNR and CNR values are calculated for the GLUE and GLUE2 results of the landmarks 2, 5, and 6. These values are measured using the windows of size 8mmx3mm in the subcutis fat (target) and gel pad (background). The average SNR values are 6.67 and 7.31, and average CNR values are 7.35 and 9.19 for the GLUE and GLUE2 methods respectively. According to these results, the proposed method outperforms the previous work, GLUE.

4. CONCLUSION

In this paper, we introduced a novel technique for calculating the strain images by estimating time delay between two frames of RF data. We proposed a novel method that utilizes the second-order derivative of the data term to improve the quality of the displacement estimation. We further introduced the ESM optimization technique in the ultrasound elastography field. Our technique is global and estimates the

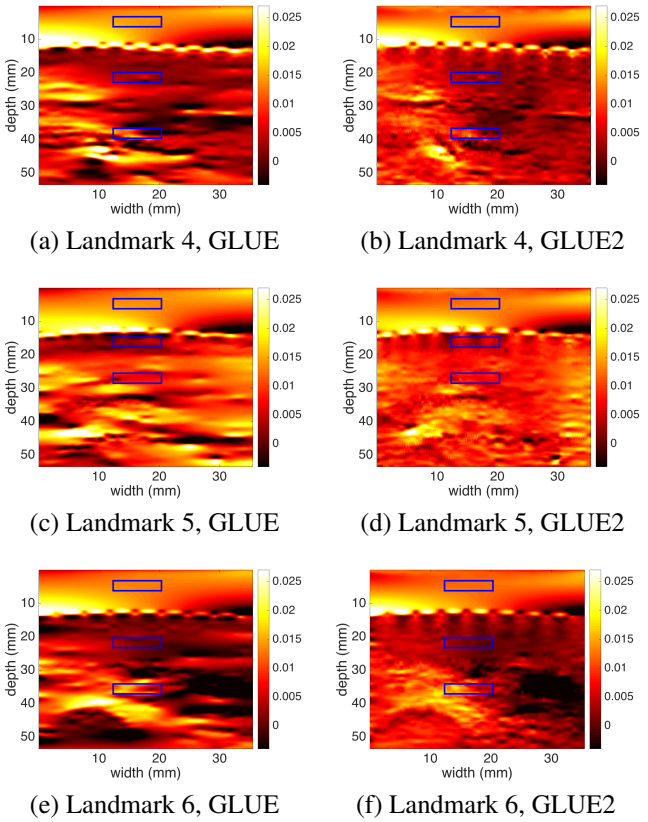

(a) Landmark 4, GLUE (b) Landmark 4, GLUE2

(c) Landmark 5, GLUE (d) Landmark 5, GLUE2

(e) Landmark 6, GLUE (f) Landmark 6, GLUE2

Fig. 2. Strain images of the affected arm at different locations.

2D displacement field of the entire image simultaneously, and is further highly suitable for real-time elastography. We further introduced the application of quasi-static ultrasound elastography for detection of lymphedema. We proposed the biomarker of SR (Strain Ratio), and showed that it is consistently different in the affected and healthy arms. Future work will focus on applying GLUE2 to data from more patients to test the observations of this study.

ACKNOWLEDGEMENTS

The authors thank Dr. Louis G. Johnson Foundation and PERFORM Centre Equipment Grant for funding this project, and the Richard and Edith Strauss Canada Foundation for funding Hoda S. Hashemi. We also would like to thank technical help from Julian Lee from Alpinion USA.

5. REFERENCES

[1] A. G. Warren, H. Brorson, L. J. Borud, and S. A. Slavin, "Lymphedema: a comprehensive review," *Annals of plastic surgery*, vol. 59, no. 4, pp. 464–472, 2007.

[2] C. C. Schook, J. B. Mulliken, S. J. Fishman, F. D. Grant, D. Zurakowski, and A. K. Greene, "Primary lymphedema: clinical features and management in 138 pe-

diatric patients," *Plastic and reconstructive surgery*, vol. 127, no. 6, pp. 2419–2431, 2011.

[3] C. Lim, H. Seo, K. Kim, S. Chung, and K. Seo, "Measurement of lymphedema using ultrasonography with the compression method," *Lymphology*, vol. 44, no. 2, p. 72, 2011.

[4] I. ISL, "The diagnosis and treatment of peripheral lymphedema," *Lymphology*, vol. 36, no. 2, pp. 84–91, 2003.

[5] E. Fumiere, O. Leduc, S. Fourcade, C. Becker, C. Garbar, R. Demeure, F. Wilputte, A. Leduc, and C. Delcour, "Mr imaging, proton mr spectroscopy, ultrasonographic findings in patients with chronic lymphedema," *Lymphology*, vol. 40, no. 4, pp. 157–162, 2007.

[6] R. Righetti, B. S. Garra, L. M. Mobbs, C. M. Kraemer-Chant, J. Ophir, and T. A. Krouskop, "Feasibility of using poroelastographic for distinguishing between normal and lymphedematous tissues in vivo," *Physics in medicine and biology*, vol. 52, no. 21, p. 6525, 2007.

[7] G. P. Berry, J. C. Bamber, P. S. Mortimer, N. L. Bush, N. R. Miller, and P. E. Barbone, "The spatio-temporal strain response of oedematous and nonoedematous tissue to sustained compression in vivo," *Ultrasound in medicine & biology*, vol. 34, no. 4, pp. 617–629, 2008.

[8] L. Coutts, N. Miller, P. Mortimer, and J. Bamber, "Investigation of in vivo skin stiffness anisotropy in breast cancer related lymphoedema," *Journal of biomechanics*, vol. 49, no. 1, pp. 94–99, 2016.

[9] W. Kim, S. Chung, T. Kim, and K. Seo, "Measurement of soft tissue compliance with pressure using ultrasonography," *Lymphology*, vol. 41, no. 4, p. 167, 2008.

[10] F. Hacard, L. Machet, A. Caille, V. Tauveron, G. Georgescou, I. Rapeneau, M. Samimi, F. Patat, and L. Vaillant, "Measurement of skin thickness and skin elasticity to evaluate the effectiveness of intensive decongestive treatment in patients with lymphoedema: a prospective study," *Skin Research and Technology*, vol. 20, no. 3, pp. 274–281, 2014.

[11] R. H. Mellor, N. L. Bush, A. W. Stanton, J. C. Bamber, J. R. Levick, and P. S. Mortimer, "Dual-frequency ultrasound examination of skin and subcutis thickness in breast cancer-related lymphedema," *The breast journal*, vol. 10, no. 6, pp. 496–503, 2004.

[12] J. Ophir, S. Alam, B. Garra, F. Kallel, E. Konofagou, T. Krouskop, and T. Varghese, "Elastography: ultrasonic estimation and imaging of the elastic properties of tissues," *Proceedings of the Institution of Mechanical Engineers, Part H: Journal of Engineering in Medicine*, vol. 213, no. 3, pp. 203–233, 1999.

[13] T. J Hall, P. E Barboneg, A. A Oberai, J. Jiang, J.-F. Dord, S. Goenezen, and T. G Fisher, "Recent results in nonlinear strain and modulus imaging," *Current medical imaging reviews*, vol. 7, no. 4, pp. 313–327, 2011.

[14] H. Rivaz, E. M. Boctor, M. A. Choti, and G. D. Hager, "Ultrasound elastography using multiple images," *Medical image analysis*, vol. 18, no. 2, pp. 314–329, 2014.

[15] M. G. Kibria and M. K. Hasan, "A class of kernel based real-time elastography algorithms," *Ultrasonics*, vol. 61, pp. 88–102, 2015.

[16] J. Jiang and T. J. Hall, "A coupled subsample displacement estimation method for ultrasound-based strain elastography," *Physics in medicine and biology*, vol. 60, no. 21, p. 8347, 2015.

[17] C. Lim and et al, "Optimal pressure for measuring objective lymphedema with postoperative ultrasonography in patients with breast cancer," *Computer Assisted Surgery*, vol. 21, no. sup1, pp. 102–110, 2016.

[18] S. Benhimane and E. Malis, "Real-time image-based tracking of planes using efficient second-order minimization," in *Intelligent Robots and Systems*, vol. 1. IEEE, 2004, pp. 943–948.

[19] H. S. Hashemi and H. Rivaz, "Global time-delay estimation in ultrasound elastography," *IEEE Transactions on Ultrasonics, Ferroelectrics, and Frequency Control*, vol. 64, no. 10, pp. 1625–1636, 2017.

[20] H. Rivaz, E. M. Boctor, M. A. Choti, and G. D. Hager, "Real-time regularized ultrasound elastography," *Medical Imaging, IEEE Transactions on*, vol. 30, no. 4, pp. 928–945, 2011.

[21] C. Mei, S. Benhimane, E. Malis, and P. Rives, "Efficient homography-based tracking and 3-d reconstruction for single-viewpoint sensors," *IEEE Transactions on Robotics*, vol. 24, no. 6, pp. 1352–1364, 2008.

[22] C. Wachinger, P. Golland, C. Magnain, B. Fischl, and M. Reuter, "Multi-modal robust inverse-consistent linear registration," *Human brain mapping*, vol. 36, no. 4, pp. 1365–1380, 2015.

[23] H. Zhou and H. Rivaz, "Registration of pre-and postresection ultrasound volumes with noncorresponding regions in neurosurgery," *IEEE journal of biomedical and health informatics*, vol. 20, no. 5, pp. 1240–1249, 2016.